# Analysis and Design of Miniaturized Lumped-Distributed Impedance-Transforming Baluns

Kian Sen Ang, *Member, IEEE*, Yoke Choy Leong, and Chee How Lee

***Abstract*—Conventional distributed baluns employ $\lambda/2$ transmission lines or $\lambda/4$ coupled lines. By adding only one or two lumped capacitors, the required coupled-line lengths of a new balun structure can be made as short as $\lambda/24$. Design curves for these miniaturized impedance-transforming baluns are derived using a systematic even- and odd-mode analysis technique. This approach also provides valuable insight into the tradeoffs between coupled-line lengths, number of capacitors, bandwidth, and impedance-transforming ratios. Experimental results of a single-capacitor balun with $\lambda/9$ coupled lines and a two-capacitor balun with $\lambda/24$ coupled lines will be presented. Both baluns achieved 0.5-dB amplitude balance and 5° phase balance, with over 10-dB return loss from 1.1 to 1.6 GHz.**

***Index Terms*—Baluns, distributed, impedance transformation, lumped, miniature.**

## I. Introduction

BALUNS ARE key components in balanced circuit topologies such balanced mixers, frequency multipliers, and push–pull amplifiers. Recently, it has also been shown that baluns can be used to form 180° hybrids [1], which further widens their applications. Various balun configurations have been reported for applications in microwave integrated circuits (MICs) and monolithic microwave integrated circuits (MMICs) [2]–[10]. Many of these structures, however, are not well suited for wireless applications operating in the lower microwave region.

Most balun configurations employ either distributed or lumped elements. Distributed baluns consist of sections of transmission lines [2], [3] or coupled lines [4], which are $\lambda/2$ or $\lambda/4$ long at the center frequency of operation. These structures occupy large circuit areas, except at very high frequencies. For lower frequency applications, these $\lambda/4$ line sections can be made more compact by meandering the lines [5] or by replacing them with inter-wound spiral transformers [6]–[8]. However, this results in increased design complexity, as these structures need to be modeled using electromagnetic simulations or characterized based on measurements [7], [8]. Many of these distributed baluns also require some nonplanar or multilayer structures that are not widely applicable [4]–[8]. Lumped-element baluns employing low-pass high-pass filter structures have also been demonstrated [9], [10]. Unfortunately, these structures require many lumped components and often exhibit poor balun balance across frequency. Therefore, it will be highly desirable to have a compact planar balun structure with low component count for high yield and low-cost production required by the wireless and mobile communications market.

Recently, balun structures employing both lumped and distributed elements have been proposed [11]–[13]. The addition of lumped elements reduces the required coupled-line lengths to much smaller than $\lambda/4$. The balun structure proposed by Ojha *et al.* [11] and Kumar *et al.* [12] employs only one coupled section with two capacitors, but the balun does not exhibit optimal performance in terms of input matching and output balance variations with frequency. Another lumped-distributed balun described by Tang and Chang [13] exhibits good balun performance, but it requires four capacitors with two coupled-line sections. Moreover, not much design information is available, as these baluns were designed using empirical methods of circuit optimization, parametric analysis [11], [12], or electromagnetic simulations [13]. In this paper, a systematic approach based on even- and odd-mode analysis techniques is employed. This provides valuable insights into the limitations and design requirements of these balun structures. It also suggests the optimal placement of lumped capacitors for effective shortening of the coupled-line lengths. Consequently, this leads to the introduction of a new lumped-distributed balun structure employing two coupled-line sections whose length can be shortened using only one or two capacitors. Various design curves, including designs with impedance transformation between the unbalanced and balanced ports, will be derived. Based on these design curves, the tradeoffs between coupled-line length, number of capacitors, bandwidth, and impedance-transforming ratio also become apparent. The design and performance of these new miniaturized balun structures will be presented in this paper.

## II. Analysis

The baluns described in this paper are composed of a symmetrical four-port network where one of the ports is terminated with a short or open circuit, as shown in Fig. 1. It provides balanced outputs to load admittances $Y_{\rm out}$ from an unbalanced input with source admittance $Y_{\rm in}$. In general, the admittances $Y_{\rm in}$ and $Y_{\rm out}$ are different. Thus, in addition to providing balanced outputs, the balun also needs to perform impedance transformation between the source and load admittances.

Manuscript received June 20, 2002; revised November 13, 2002.

The authors are with the DSO National Laboratories, Singapore 118230 (e-mail: akiansen@dso.org.sg).

Digital Object Identifier 10.1109/TMTT.2003.808677

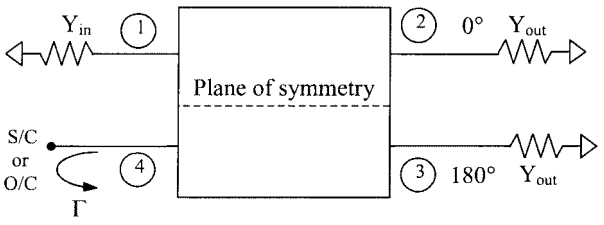


Fig. 1. Balun configured as a symmetrical four-port network with one port terminated in a short or open circuit.

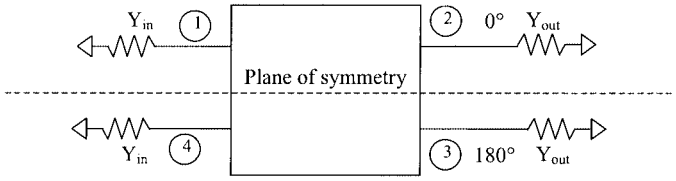


Fig. 2. Corresponding symmetrical four-port network for even- and odd- mode analysis.

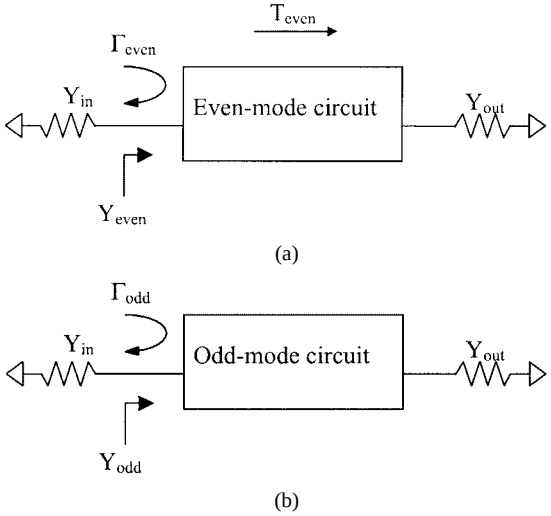


Fig. 3. (a) Even-mode circuit and (b) odd-mode circuit of the corresponding symmetrical four-port network in Fig. 2.

With the port assignments defined in Fig. 1, the $S$-parameters characterizing the balun operation are given by

$$S_{21} = -S_{31} \tag{1a}$$

$$S_{11} = 0. \tag{1b}$$

This balun configuration can be analyzed using the even- and odd-mode analysis technique previously described [14]. In this approach, the open- or short-circuited terminal is replaced by a load $Y_{\text{in}}$ to form a fully symmetrical network, as shown in Fig. 2. This facilitates the decomposition of the network into even- and odd-mode circuits, shown in Fig. 3(a) and (b), respectively. It can be shown [14] that (1) will be satisfied when the transmission and reflection coefficients in the even- and odd-mode circuits of Fig. 3 are given by the following.

To satisfy (1a)

$$\frac{T_{\text{even}}(1-\Gamma_{\text{odd}}\Gamma)}{2-\Gamma(\Gamma_{\text{even}}+\Gamma_{\text{odd}})} = 0. \tag{2a}$$

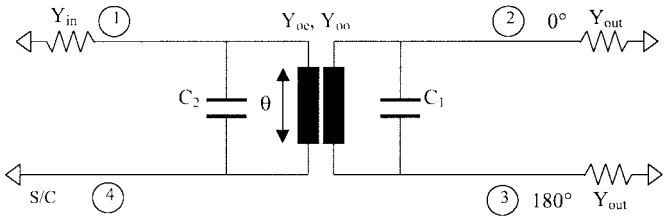


Fig. 4. Schematic diagram of the balun previously proposed balun by Ojha *et al.* [11].

To satisfy (1b)

$$\frac{\Gamma_{\text{even}}+\Gamma_{\text{odd}}-2\Gamma_{\text{even}}\Gamma_{\text{odd}}\Gamma}{2-\Gamma(\Gamma_{\text{even}}+\Gamma_{\text{odd}})} = 0. \tag{2b}$$

Provided the denominators in (2) are not zero, these equations can be simplified by substituting $Y_{\text{even}}$, $Y_{\text{odd}}$, and $Y_{\text{in}}$, defined in Fig. 3, into $\Gamma_{\text{even}}$ and $\Gamma_{\text{odd}}$ as follows:

$$T_{\text{even}} = 0 \tag{3a}$$

$$Y_{\text{even}} + Y_{\text{odd}} = 2Y_{\text{in}} \text{ for the short-circuit case where } \Gamma = -1 \tag{3b}$$

$$\frac{1}{Y_{\text{even}}} + \frac{1}{Y_{\text{odd}}} = \frac{2}{Y_{\text{in}}} \text{ for the open-circuit case where } \Gamma = 1. \tag{3c}$$

These equations state the requirements of the even- and odd-mode circuits for the balun operation. Specifically, (3a) shows that, to achieve perfect amplitude and phase balance, the balun has to present a transmission stop in the even-mode circuit. In addition, (3b) shows that, to achieve perfect matching at the balun input in the short-circuit case, the sum of the even- and odd-mode admittances must be twice the source admittance. Conversely, for the open-circuit case, shown in (3c), the sum of the even- and odd-mode impedances must be twice the source impedance.

With these valuable insights, the limitations and design requirements of the previously proposed balun structures [11], [13] can be evaluated. Furthermore, a new balun structure with optimum characteristics in terms of balun performance and number of capacitors employed is proposed.

Fig. 4 shows the schematic diagram of the balun structure previously proposed by Ojha *et al.* [11], which employs a short-circuited termination at port 4. It consists of a coupled-line section of electrical length $\theta$, with even- and odd-mode admittances given by $Y_{oe}$ and $Y_{oo}$, respectively. Lumped capacitors $C_1$ and $C_2$ are added on both sides of the coupled line to effectively increase the electrical length of the coupled lines such that $\theta$ is typically much less than $\lambda/4$.

The even- and odd-mode circuits of the balun are shown in Fig. 5(a) and (b), respectively. In the even mode, the balun consists of a coupled-line section with electrical length $\theta/2$, which is open circuited. In the odd mode, this coupled-line section is short circuited with two shunt capacitors $2C_1$ and $2C_2$. At the designed frequency of operation, the even-mode circuit has to be a transmission stop, while the odd-mode circuit has to transform $Y_{\text{out}}$ to the required $Y_{\text{odd}}$ specified by (3b).

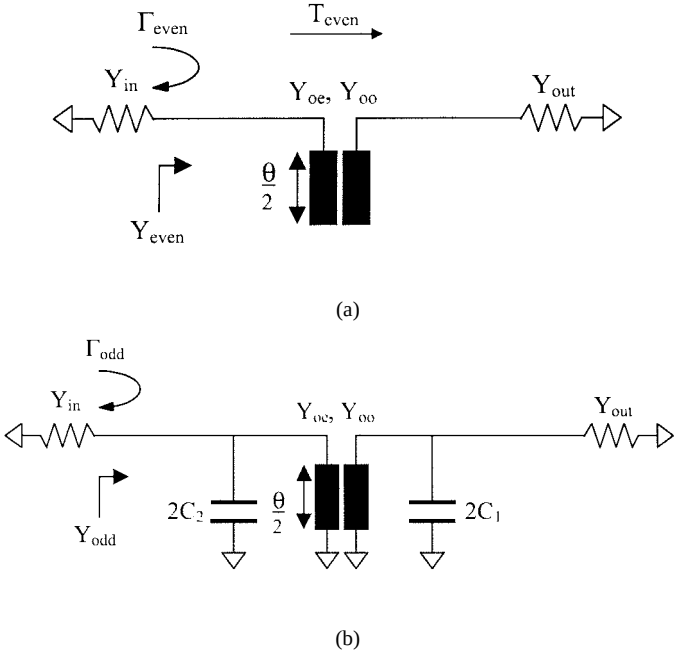


Fig. 5. (a) Even-mode circuit and (b) odd-mode circuit of the previously proposed balun in Fig. 4.

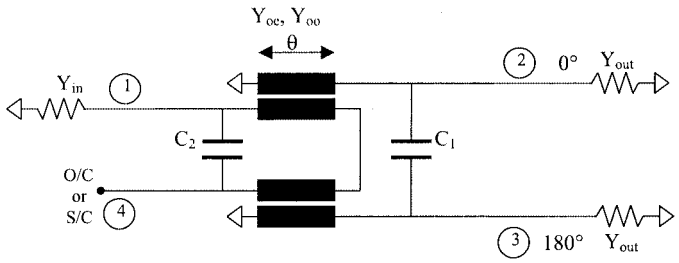


Fig. 6. Schematic diagram of the newly proposed lumped-distributed balun.

From (3a), the even-mode circuit has to present an ideal transmission stop to achieve perfect amplitude and phase balance. Although the structure in Fig. 5(a) has been described as an all-stop filter structure [15], an ideal transmission stop is only achieved when $\theta/2$ equals $\lambda/4$. When $\theta/2$ is less than $\lambda/4$, there is a finite level of even-mode transmission, causing amplitude and phase imbalance. Although these imbalances can be minimized by setting $Y_{oe}$ and $Y_{oo}$ such that the even-mode transmission is small, perfect amplitude and phase balance cannot be achieved.

In this paper, a balun structure with amplitude and phase balances that are theoretically perfect and frequency independent is presented. Its schematic is shown in Fig. 6. The coupled-line section of the previous balun has been replaced by two coupled-line sections, which are short circuited at one end. For this structure, port 4 may be terminated in a short or open circuit. Fig. 7(a) and (b) shows the corresponding even- and odd-mode circuits. Unlike the structure in Fig. 5(a), the even-mode circuit in Fig. 7(a) presents a perfect transmission stop that is frequency independent for all values of $\theta$. Therefore, theoretically perfect and frequency-independent amplitude and phase balance of the proposed balun is ensured. For the odd-mode circuit in Fig. 7(b),

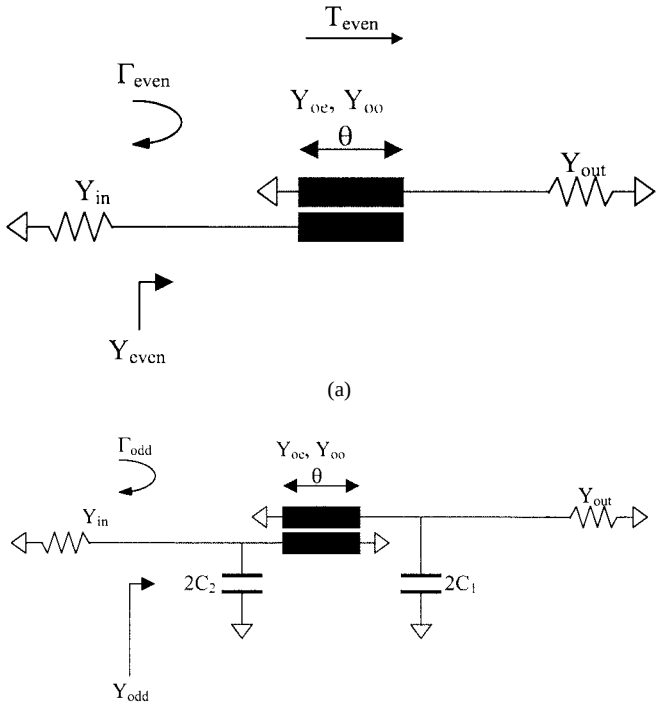


Fig. 7. (a) Even-mode circuit and (b) odd-mode circuit of the newly proposed balun in Fig. 6.

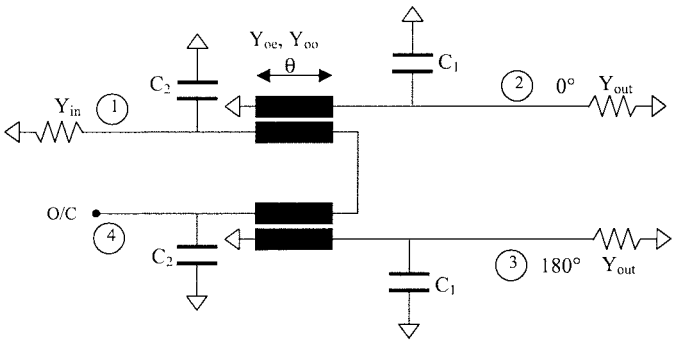


Fig. 8. Schematic diagram of the balun previously proposed by Tang and Chang [13].

the circuit parameters are designed such that $Y_{\rm odd}$ satisfies either (3b) for the short-circuit case or (3c) for the open-circuit case.

It is instructive at this point to compare the new balun structure with that of Fig. 8, which was previously described by Tang and Chang [13]. It employs an open-circuit termination at port 4 with four shunt capacitors. Fig. 9(a) and (b) shows the corresponding even- and odd-mode circuits. Comparing with Fig. 7(a), the even-mode circuit in Fig. 9(a) has the same coupled-line section with two additional shunt capacitors. Unlike the odd-mode capacitors, which serve to shorten the coupled-line lengths, these additional even-mode capacitors are not necessary for the balun operation. The odd-mode circuits in Figs. 7(b) and 9(b) are identical, except that capacitor values in Fig. 7(b) are twice that of Fig. 9(b). Therefore, the new balun structure presents a more optimal placement of the capacitors,

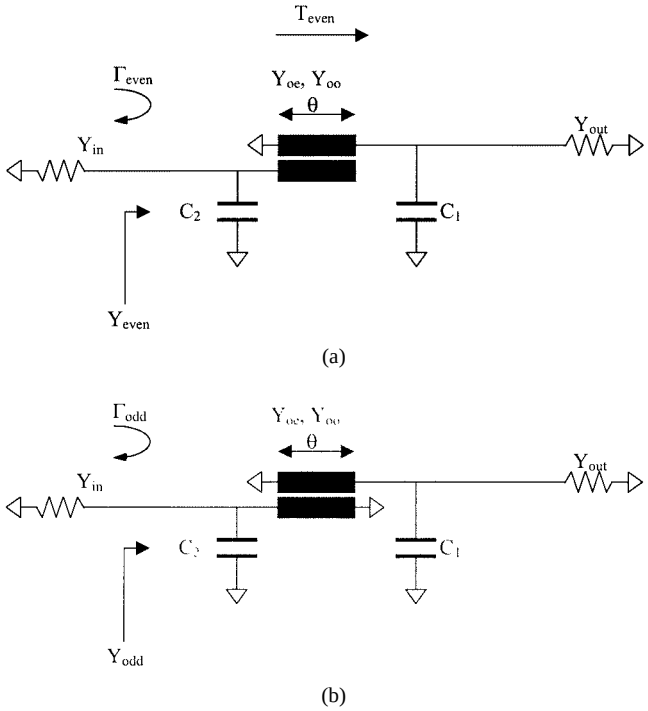


Fig. 9. (a) Even-mode circuit and (b) odd-mode circuit of the previously proposed balun in Fig. 8.

as it requires fewer capacitors and half the capacitance value for each capacitor. Practically, this implies lower production cost and smaller circuit areas. In fact, it will be shown in the following section that significant reduction in coupled-line length can be obtained by using only a single capacitor.

## III. Design

In this section, design equations for the new impedance-transforming balun structure in Fig. 6 will be derived. Only the case where a short circuit is employed at port 4 will be considered, as the same approach can applied to the other previously described balun configurations.

Referring to Fig. 7(b), the circuit parameters $Y_{oe}$, $Y_{oo}$, $C_1C_2$, and $\theta$ are chosen such that (3b) is satisfied. The even- and odd-mode admittances in (3b) can be determined to be

$$Y_{\text{even}} = j\frac{(Y_{oe}+Y_{oo})\tan\theta}{2} \tag{4a}$$

$$Y_{\text{odd}} = j2wc_2 + Y_{11} - \frac{Y_{12}Y_{21}}{Y_{22}+(j2wc_1+Y_{\text{out}})} \tag{4b}$$

where

$$Y_{11} = Y_{22} = -j\frac{Y_{oo}+Y_{oe}}{2\tan\theta} \tag{5a}$$

$$Y_{12} = Y_{21} = -j\frac{Y_{oo}-Y_{oe}}{2\sin\theta}. \tag{5b}$$

By substituting (4a) and (b) into (3b), and equating the real and imaginary parts, the following equations can be obtained.

Equating the real part

$$\left(\frac{Y_{\text{out}}}{Y_{\text{in}}}\right)(Y_{oo}-Y_{oe})^2 - (8\sin^2\theta) \times \left(Y_{\text{out}}^2 + \left(\frac{Y_{oo}+Y_{oe}}{2\tan\theta} - 2wc_1\right)^2\right) = 0. \tag{6a}$$

Equating the imaginary part

$$\underbrace{(Y_{oo}+Y_{oe})}_{\text{First term}}\underbrace{\left(\tan\theta + \frac{1}{\tan\theta}\left(\frac{2Y_{\text{in}}}{Y_{\text{out}}}-1\right)\right)}_{\text{Second term}} + \underbrace{4\left(wc_2 - \left(\frac{2Y_{\text{in}}}{Y_{\text{out}}}\right)wc_1\right)}_{\text{Last term}} = 0. \tag{6b}$$

Equations (6a) and (6b) can be solved for $Y_{oe}$ and $Y_{oo}$ to give

$$Y_{oe} = F(\theta, wc_1, wc_2, Y_{\text{in}}, Y_{\text{out}}) = \frac{1}{Z_{oe}} \tag{7a}$$

$$Y_{oo} = G(\theta, wc_1, wc_2, Y_{\text{in}}, Y_{\text{out}}) = \frac{1}{Z_{oo}} \tag{7b}$$

where $F$ and $G$ are functions of $\theta$, $\omega c_1$, $\omega c_2$, $Y_{\text{in}}$, and $Y_{\text{out}}$.

Based on the solutions for $Z_{oe}$ and $Z_{oo}$ in (7), various design curves for the new balun structure can be obtained. We will first consider the case of a 50-$\Omega$ system, where $Y_{\text{in}} = Y_{\text{out}} = 0.02$ mhos. In this case, no impedance transformation is involved and (6b) reduces to

$$(Y_{oo}+Y_{oe})\left(\tan\theta + \frac{1}{\tan\theta}\right) + 4wc_2 - 8wc_1 = 0. \tag{8}$$

To satisfy (8), it is clear that capacitor $C_1$ is required, while capacitor $C2$ can be set to zero. However, it will be shown that the presence of $C2$ can further reduce the value of $\theta$ required. The solutions of solutions of $Z_{oe}$ and $Z_{oo}$ are plotted in Figs. 10 and 11 for various $\omega c_1$ values. In Fig. 10, the value of $\omega c_2$ is set to 0 mho, i.e., when only one capacitor $C_1$ is employed. It can be seen that the balun can be realized by a wide range of practical values for $Z_{oe}$ and $Z_{oo}$ with $\theta$ between 20° and 60° depending on the value of $\omega c_1$. Generally, the required $Z_{oe}$ and $Z_{oo}$ decreases with increasing $\omega c_1$. For each $\omega c_1$ value, there exist a minimum value of $Z_{oe}$, which occurs when $\theta$ is around 40°, and $Z_{oe}$ increases rapidly as $\theta$ deviates from 40°. On the other hand, $Z_{oo}$ decreases monotonically with increasing $\theta$, where the decrease is highly rapid when $\theta$ is small and gradually levels off when $\theta$ is approximately 20°.

It should be noted that these curves represent solutions at the center frequency and each has a different passband characteristic. In general, solutions with larger $Z_{oe}$ exhibit wider bandwidths. For the same $Z_{oe}$, the solutions at the minimum points of the $Z_{oe}$ curves exhibit a more symmetrical response. This is illustrated in Fig. 12(a)–(c), which plot the frequency responses at points, A–A', B–B', and C–C', respectively, in Fig. 10. These

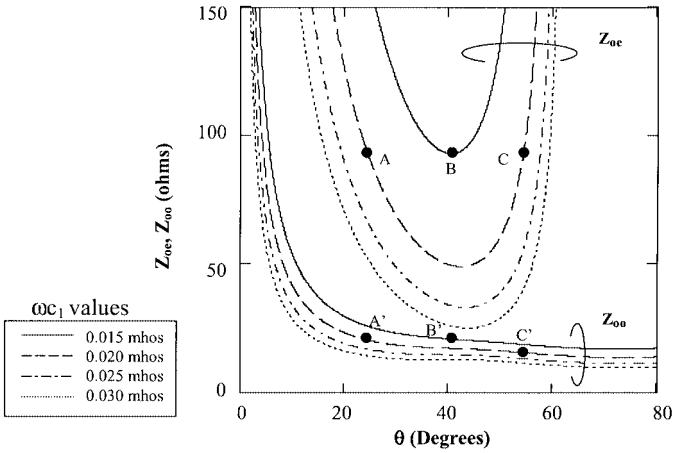


Fig. 10. Design curves for determining $Z_{oe}$, $Z_{oo}$, and $\theta$ for various $\omega c_1$ values with $\omega c_2 = 0$ mho and $Y_{\text{in}} = Y_{\text{out}} = 0.02$ mho.

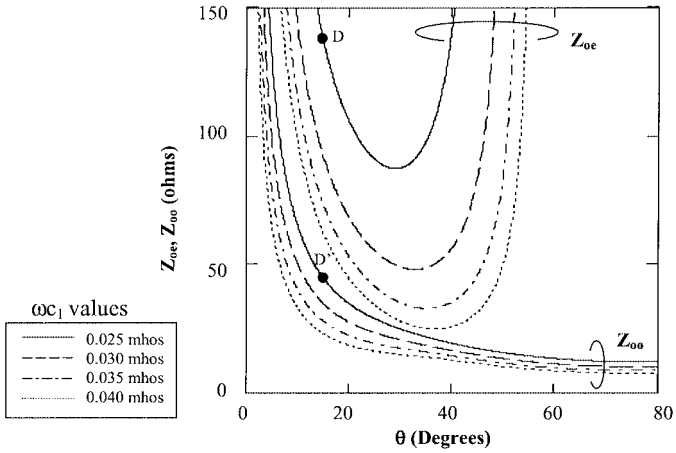


Fig. 11. Design curves for determining $Z_{oe}$, $Z_{oo}$, and $\theta$ for various $\omega c_1$ values with $\omega c_2 = 0.02$ mhos and $Y_{\text{in}} = Y_{\text{out}} = 0.02$ mho.

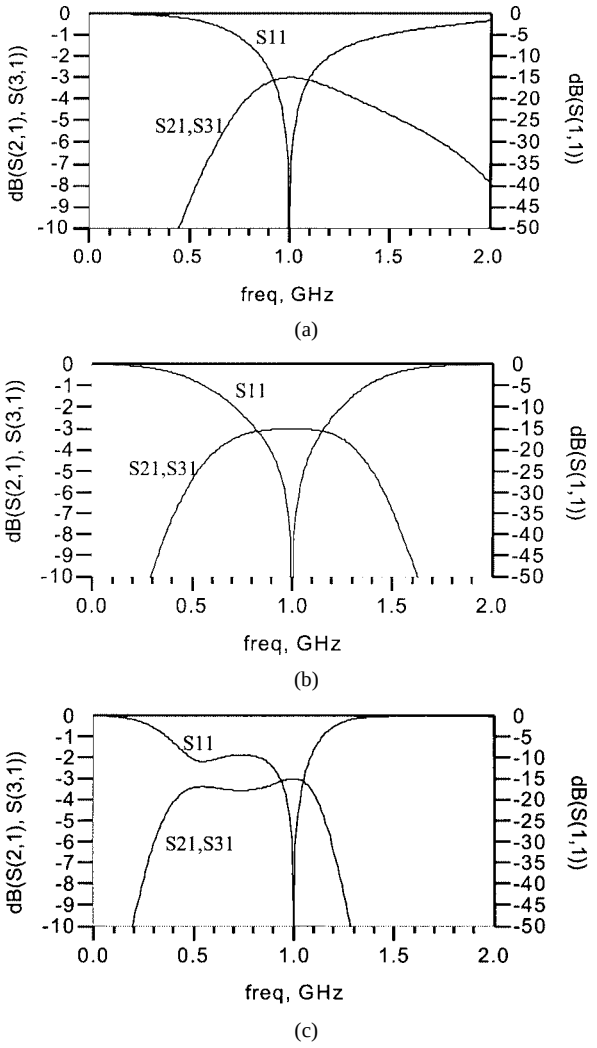


Fig. 12. (a) Simulated frequency response for solution at point A in Fig. 10. (b) Simulated frequency response for solution at point B in Fig. 10. (c) Simulated frequency response for solution at point C in Fig. 10.

are obtained using an *HP-ADS*[1] circuit simulator based on ideal circuit elements. The designed frequency is at 1 GHz. Comparing the three plots, Fig. 12(a) exhibits a relatively narrow bandwidth. Although the passband in Fig. 12(c) is relatively wider, it has a nonsymmetrical return-loss characteristic where the null is located at the upper end of the passband. Fig. 12(b) exhibits a more optimal response in that it has a symmetrical passband with the return loss null centered at the mid-band.

Fig. 11 plots the solutions for the case when both capacitors $C_1$ and $C_2$ are employed and $\omega c_2$ is set to 0.05 mho. It can be seen that the presence of $C_2$ shifts the $Z_{oe}$ curves toward the left-hand side, where the range of $\theta$ is now between 10° and 50°. Therefore, the addition of $C_2$ results in a reduction in the balun size. Similar to the previous case, solutions with larger $Z_{oe}$ exhibits larger bandwidth and there is an optimum solution for each $\omega c_1$ value having a symmetrical response. However, these solutions may not be located at the minimum of the $Z_{oe}$ curves, as in the previous case. For example, when $\omega c_1$ is 0.02 mho, a solution with a symmetrical response was found at point D–D' in Fig. 11.

[1]*Agilent Advanced Design System (ADS)*, ver. 1.3, Agilent Technol., Palo Alto, CA.

While it has been shown that additional capacitors result in smaller baluns, it is also important to assess its effect on the balun's operational bandwidth. Fig. 13 plots the simulated frequency response of the two-capacitor balun using the solution at point D in Fig. 11 and the single-capacitor balun using the solution at point B in Fig. 10. Also plotted is the frequency response of the conventional Marchand balun using $\lambda/4$ coupled sections with $Z_{oe} = 97\,\Omega$ and $Z_{oo} = 26\,\Omega$, as given in [1]. Although the bandwidths of each of these baluns depend on the particular solution set chosen, as illustrated in Fig. 12, the results in Fig. 13 are indicative of the relative bandwidths that can be achieved. In general, the conventional Marchand balun employing $\lambda/4$-coupled sections exhibits the widest bandwidth, as shown in Fig. 13(c). As the coupled sections are shortened to $\lambda/9$ with the addition of one capacitor, the 10-dB return-loss bandwidth is reduced by approximately 20% in Fig. 13(b). When the coupled sections are further shortened to $\lambda/24$ using two capacitors, the bandwidth is reduced by approximately 40% in Fig. 13(a). Therefore, it is apparent that there is a tradeoff between the size and bandwidth of the balun.

We will now consider the case where impedance transformation is required. In this case, three sets of design curves can be

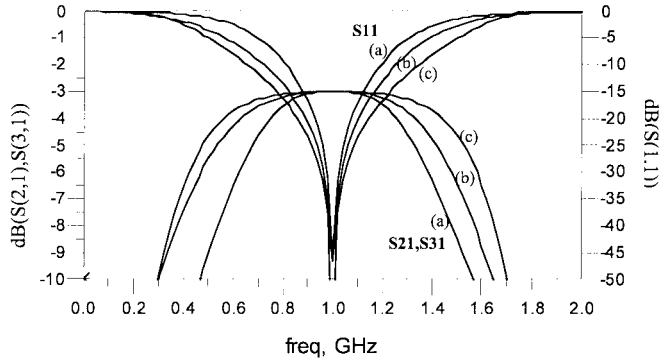


Fig. 13. Simulated frequency responses for the three baluns. (a) Miniaturized two-capacitor balun using solution at point D in Fig. 11. (b) Miniaturized single-capacitor balun using solution at point B in Fig. 10. (c) Conventional Marchand balun using $Z_{oe} = 97\ \Omega$ and $Z_{oo} = 26\ \Omega$ given in [1].

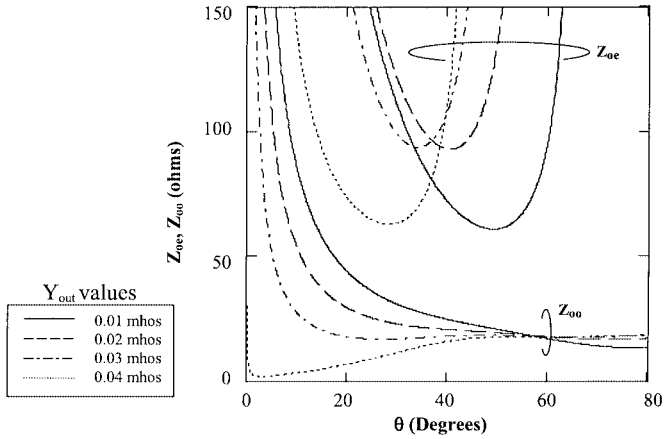


Fig. 14. Design curves for determining $Z_{oe}$, $Z_{oo}$, and $\theta$ for various $Y_{\text{out}}$ values with $Y_{\text{in}} = 0.02$ mho, $\omega c_1 = 0.015$ mho, and $\omega c_2 = 0$ mho.

identified, as illustrated in Figs. 14–16. Fig. 14 plots the solutions of $Z_{oe}$ and $Z_{oo}$ for transformation ratios $(Y_{\text{out}}/Y_{\text{in}}) \leq 2$. Solutions for transformation ratios >2 are plotted in Figs. 15 and 16.

When $(Y_{\text{out}}/Y_{\text{in}}) \leq 2$, the second term in (6b) is positive for all values of $\theta$ in the range $0° < \theta < 90°$. The first term is also positive for positive solutions of $Y_{oe}$ and $Y_{oo}$. Therefore, to satisfy the equation, $\omega c_1$ and $\omega c_2$ have to be chosen such that the last term is negative. Although this will ensure that the sum of $Y_{oe}$ and $Y_{oo}$ is positive, a judicious choice of $\omega c_1$ and $\omega c_2$ is required to ensure that both $Y_{oe}$ and $Y_{oo}$ are positive. In Fig. 14, $\omega c_1$ and $\omega c_2$ are set at 0.015 and 0 mho, respectively. The value of $Y_{\text{in}}$ is fixed at 0.02 mho, while $Y_{\text{out}}$ is varied from 0.01 to 0.04 mho. It can be observed that the $Z_{oe}$ curves shifts toward smaller $\theta$ values as $Y_{\text{out}}$ is increased. Toward smaller $\theta$ values, the $Z_{oo}$ curves also shift downwards with increasing $Y_{\text{out}}$. It should be noted that no solution exists at $\theta = 0$, as both $Z_{oe}$ and $Z_{oo}$ tends to infinite values.

When $(Y_{\text{out}}/Y_{\text{in}}) > 2$, the second term in (6b) may be positive or negative, depending on the value of $\theta$.

Specifically, the second term is positive when

$$\theta > \tan^{-1}\sqrt{1 - \frac{2Y_{\text{in}}}{Y_{\text{out}}}} \tag{9a}$$

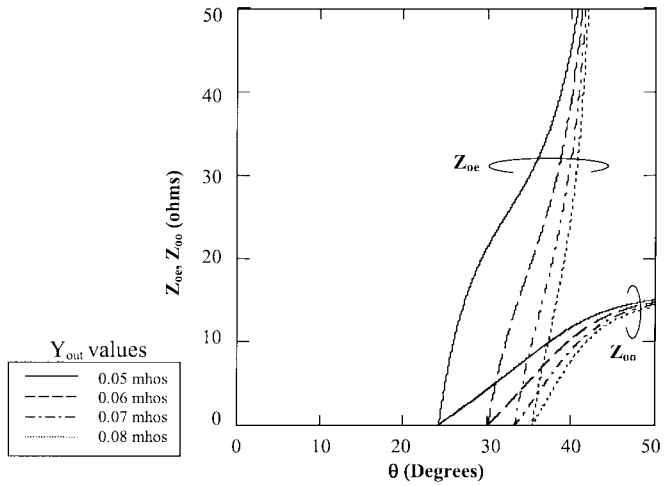


Fig. 15. Design curves for determining $Z_{oe}$, $Z_{oo}$, and $\theta$ for various $Y_{\text{out}}$ values with $Y_{\text{in}} = 0.02$ mho, $\omega c_1 = 0.02$ mho, and $\omega c_2 = 0$ mho.

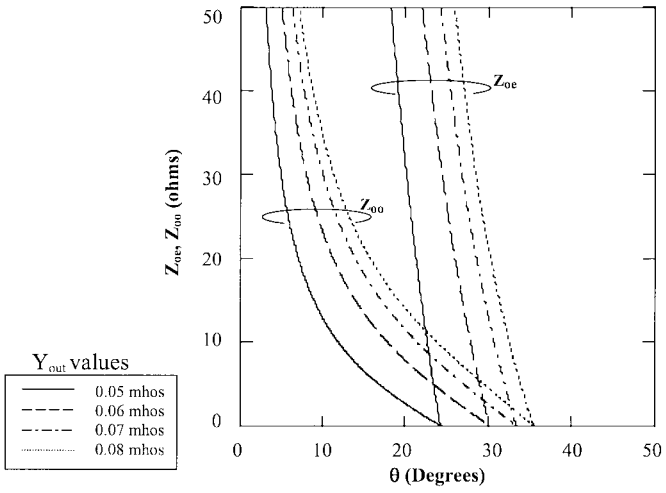


Fig. 16. Design curves for determining $Z_{oe}$, $Z_{oo}$, and $\theta$ for various $Y_{\text{out}}$ values with $Y_{\text{in}} = 0.02$ mho, $\omega c_1 = 0$ mho, and $\omega c_2 = 0.02$ mho.

and negative when

$$\theta < \tan^{-1}\sqrt{1 - \frac{2Y_{\text{in}}}{Y_{\text{out}}}}. \tag{9b}$$

For $\theta$ in the range where the second term in (6b) is positive, $\omega c_1$ and $\omega c_2$ have to be chosen such that the last term is negative and that solutions for $Y_{oe}$ and $Y_{oo}$ are both positive. Conversely, for $\theta$ in the range where the second term in (6b) is negative, $\omega c_1$ and $\omega c_2$ have to be chosen such that the last term is positive and that solutions for $Y_{oe}$ and $Y_{oo}$ are both positive. These two cases are illustrated in Figs. 15 and 16, respectively.

For both Figs. 15 and 16, $Y_{\text{in}}$ is fixed at 0.02 mho, while $Y_{\text{out}}$ is varied from 0.05 to 0.08 mho. In Fig. 15, $\omega c_1$ and $\omega c_2$ are set at 0.02 and 0 mho so that positive solutions for $Z_{oo}$ and $Z_{oe}$ are found in the range of $\theta$, as specified in (9a). Conversely, in Fig. 16, $\omega c_1$ and $\omega c_2$ are set at 0 and 0.02 mho so that positive solutions for $Z_{oo}$ and $Z_{oe}$ are found in the range of $\theta$, as specified in (9b). These curves show that with the proper selection of $\omega c_1$ and $\omega c_2$, positive values for $Z_{oo}$ and $Z_{oe}$ can be found throughout a wide range of $\theta$ values even for $(Y_{\text{out}}/Y_{\text{in}}) > 2$.

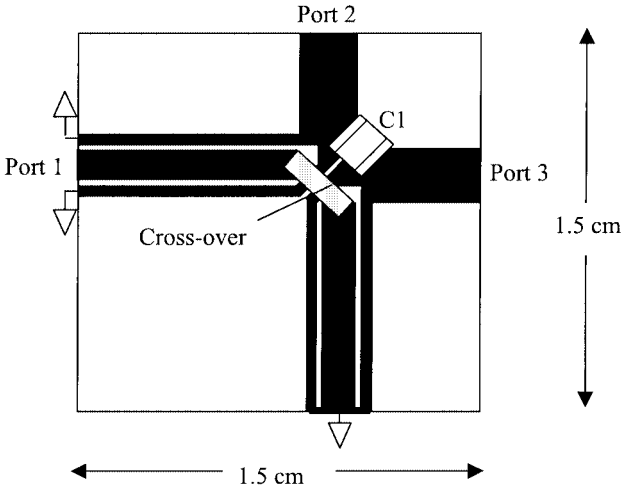


Fig. 17. Layout of the fabricated lumped-distributed balun with a single capacitor $C_1$.

## IV. Experimental Results

To evaluate the proposed balun structures and validate the analytical results, two lumped-distributed baluns were designed for a 50-Ω system, one employing a single capacitor, while the other employing two capacitors. These baluns were realized using microstrips on a low-cost FR-4 board with a dielectric constant of 4.5 and thickness of 1.5 mm. The microstrip traces are defined by a T-tech printed circuit board (PCB) router.

Fig. 17 shows the layout of the fabricated balun employing a single capacitor $C_1$. The circuit parameters are designed according to the solution at points B–B' in Fig. 10, where $Z_{oe}$, $Z_{oo}$, $\theta$, and $\omega c_1$ are 93 Ω, 21 Ω, 40°, and 0.015 mho, respectively. To achieve the tight coupling required, a three-conductor coupled line [16] was employed. The widths of the center and the two outer conductors are 1 and 0.5 mm, respectively, while the gaps between them are 0.1 mm. The length of the coupled lines is 1 cm, which is equivalent to an electrical length of 40° at 1.4 GHz. This represents a size reduction of over 50% when compared to conventional distributed baluns employing quarter-wavelength coupled lines. The capacitor value used for $C_1$ is 2 pF. The crossover was implemented by soldering a copper tape across the microstrips. The short circuits were obtained by soldering strips of copper around the edges of the substrate. Short sections of 50-Ω microstrip lines were used to extend ports 2 and 3 for measurement, resulting in an overall circuit area of approximately $1.5 \times 1.5$ cm$^2$.

Fig. 18 shows theoretical, simulated, and measured amplitude responses of the single-capacitor balun. The theoretical and simulated responses were obtained using Agilent's *ADS* circuit simulator. Ideal coupled-line elements were employed for the theoretical response, while microstrip models were used for the simulated response. All three responses are in good agreement, with an equal power split of $-3$ dB and input match obtained at the designed frequency of 1.4 GHz. Both simulated and measured response exhibit a gentler rolloff at the higher frequencies compared to the theoretical response. Theoretically, both $S_{21}$ and $S_{31}$ have identical responses. Practically, the measured $S_{21}$ and $S_{31}$ tracks each other closely with amplitude balance within 0.5 dB throughout the measured frequency range. Based on an input return loss of 10 dB, the operational bandwidth is approximately 40%.

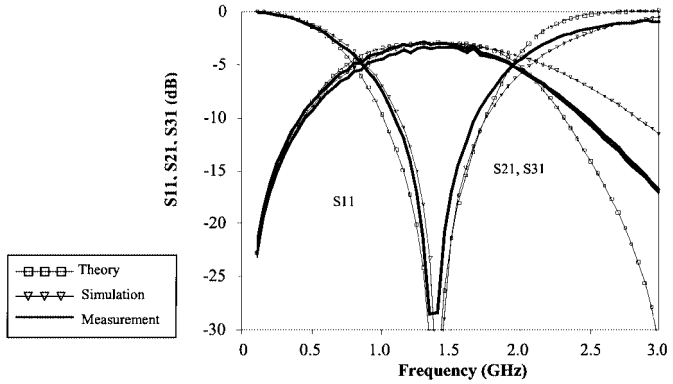


Fig. 18. Measured and theoretical amplitude balance of the single-capacitor balun.

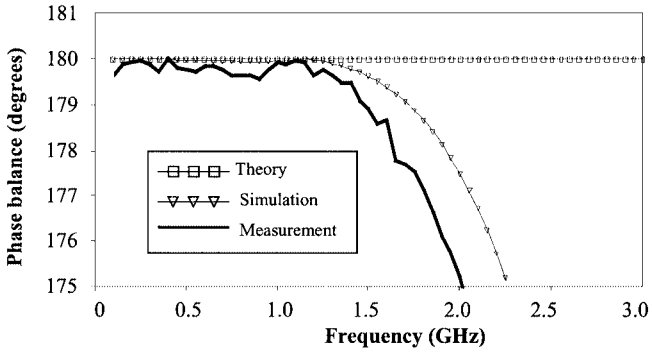


Fig. 19. Measured and theoretical phase balance of the single-capacitor balun.

Fig. 19 shows the phase balance of the single-capacitor balun. The theoretical phase balance is perfect for all frequencies. The measured phase balance is within 0.5° up to the center frequency of 1.4 GHz where it starts to degrade to 5° at 2 GHz. This can be attributed to the increasing level of even-mode transmission with increasing frequency. This is a result of forward coupling in the nonhomogenous microstrip coupled lines having unequal even- and odd-mode phase velocities. This increasing phase imbalance with frequency is also evident in the simulated response. Although this nonideality also causes amplitude imbalance, increasing amplitude imbalance is only observed at frequencies beyond 3 GHz.

The above balun has demonstrated that, by adding a single capacitor, the circuit size of conventional distributed baluns can be reduced by half. To reduce the circuit area further, a two-capacitor balun was fabricated to operate at the same frequency. The circuit layout is shown in Fig. 20. The circuit parameters are designed according to the solution at points D–D' in Fig. 11, where $Z_{oe}$, $Z_{oo}$, $\theta$, $\omega c_1$, and $\omega c_2$ are, respectively, 138 Ω, 44 Ω, 15°, 0.025 mho, and 0.02 mho. Simple parallel coupled lines, with widths of 0.5 mm and a gap of 0.15 mm, were sufficient to achieve the required coupling. The length of these coupled lines is only 5 mm. This represents a further reduction in the circuit size by half. The capacitor values used for $C_1$ and $C_2$ are 2 and 3 pF, respectively. In addition to the copper strips around the substrate edges, a via through the substrate was implemented for grounding of capacitor $C_2$. The overall circuit area is approximately $1 \times 1$ cm$^2$.

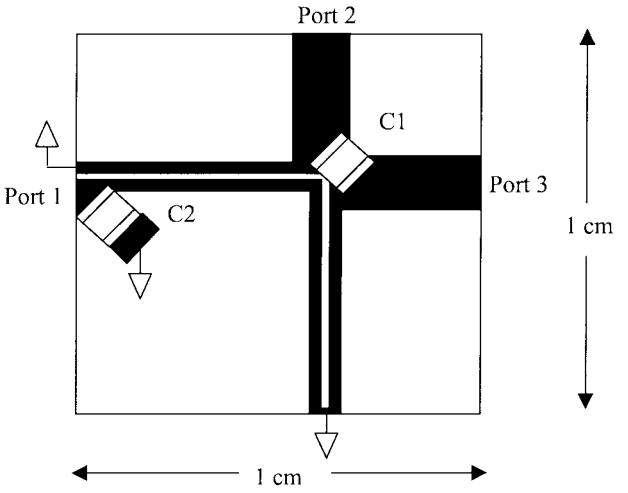


Fig. 20. Layout of the fabricated lumped-distributed balun with two capacitors $C_1$ and $C_2$.

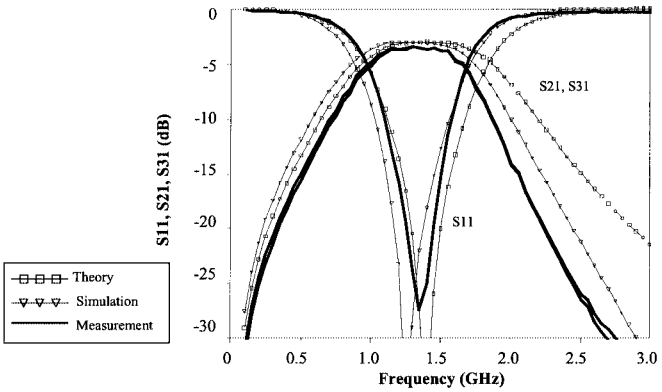


Fig. 21. Measured and theoretical amplitude response of the two-capacitor balun.

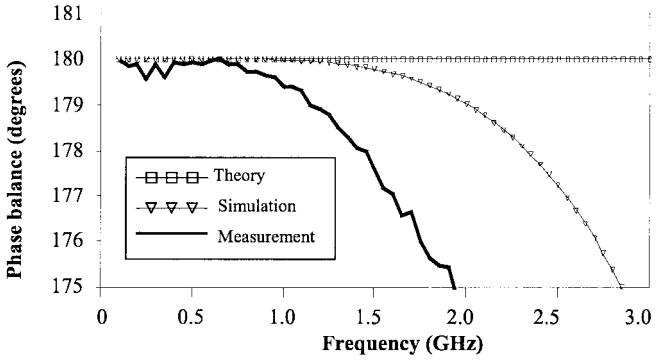


Fig. 22. Measured and theoretical phase balance of the two-capacitor balun.

The theoretical, simulated, and measured responses of the two-capacitor balun are shown in Fig. 21. Compared to single-capacitor balun response in Fig. 18, the two-capacitor balun has a slightly narrower passband with steeper band edges. The measured response exhibits a steeper high-frequency rolloff than the theoretical response. This can be attributed to the parasitic inductance of the via-hole used for grounding capacitor $C2$. This is reflected in the simulated response simulation based on microstrip coupled-line models, where a via inductance of 1 nH was included in the simulation. As in the previous balun, the measured $S_{21}$ and $S_{31}$ track each other to within 0.5 dB. Similarly, both the measured and simulated phase balance in Fig. 22 also degrade with increasing frequency, although the measured phase balance exhibits a more rapid degradation than the simulated result. Nevertheless, the phase balance is still within 5° up to 2 GHz.

## V. Conclusion

A new miniaturized lumped-distributed balun has been presented. It employs only one or two capacitors with two coupled-line sections in which the input line may be terminated in an open or short circuit. Based on a systematic even- and odd-mode analysis technique, design curves for the short-circuit case were derived. The requirement for impedance transformation has also been considered. A similar approach may be applied to the open-circuit case or to the other previously proposed lumped-distributed baluns. Improvements over these existing balun structures have also been highlighted. Tradeoffs between coupled-line length, number of capacitors, bandwidth, and impedance transforming ratio also become apparent using this approach. Using the design curves derived, two miniaturized baluns were realized. One employs a single capacitor with $\lambda/9$ coupled lines, while the other employs two capacitors with $\lambda/24$ coupled lines. Both baluns achieved 0.5-dB amplitude balance and 5° phase balance, with over 10-dB return loss from 1.1 to 1.6 GHz. These results demonstrate that these new miniaturized baluns are highly suited for wireless communication applications, which require compact structures with a low component count for high-yield and low-cost productions.

## Acknowledgment

The authors would like to thank W. L. Aw and C. K. Tay, both of Singapore Polytechnic, Singapore, for their technical support in the fabrication and measurement of the miniaturized lumped-distributed baluns.

## References

[1] K. S. Ang and Y. C. Leong, "Converting baluns into broad-band impedance-transforming 180° hybrids," *IEEE Trans. Microwave Theory Tech*, vol. 50, pp. 1190–1195, Aug. 2002.

[2] R. Sturdivant, "Balun designs for wireless, mixers amplifiers and antennas," *Appl. Microwaves*, vol. 5, pp. 34–44, Summer 1993.

[3] D. Raicu, "Design of planar, single-layer microwave baluns," in *IEEE MTT-S Int. Microwave Symp. Dig.*, 1998, pp. 801–804.

[4] A. M. Pavio and A. Kikel, "A monolithic or hybrid broadband compensated balun," in *IEEE MTT-S Int. Microwave Symp. Dig.*, 1990, pp. 483–486.

[5] K. Nishikawa, I. Toyoda, and T. Tokumitsu, "Compact and broad-band three-dimensional MMIC balun," *IEEE Trans. Microwave Theory Tech.*, vol. 47, pp. 96–98, Jan. 1999.

[6] R. H. Jansen, J. Jotzo, and M. Engels, "Improved compaction of multilayer MMIC/MCM baluns using lumped element compensation," in *IEEE MTT-S Int. Microwave Symp. Dig.*, 1997, pp. 401–404.

[7] Y. J. Yoon, Y. Lu, R. C. Frye, M. Y. Lau, P. R. Smith, L. Ahlquist, and D. P. Kossives, "Design and characterization of multilayer spiral transmission line baluns," *IEEE Trans. Microwave Theory Tech.*, vol. 47, pp. 1841–1847, Sept. 1999.

[8] Y. J. Yoon, Y. Lu, R. C. Frye, and P. R. Smith, "Modeling of monolithic RF spiral transmission line balun," *IEEE Trans. Microwave Theory Tech.*, vol. 49, pp. 393–395, Feb. 2001.

[9] H. K. Chiou, H. H. Lin, and C. Y. Chang, "Lumped-element compensated high/low-pass balun design for MMIC double-balanced mixer," *IEEE Microwave Guided Wave Lett.*, vol. 7, pp. 248–250, Aug. 1997.

[10] D. W. Lew, J. S. Park, D. Ahn, N. K. Kang, C. S. Yoo, and J. B. Lim, "A design of ceramic chip balun using the multilayer configuration," *IEEE Trans. Microwave Theory Tech.*, vol. 49, pp. 220–224, Jan. 2001.
[11] S. P. Ojha, G. R. Branner, and B. P. Kumar, "A miniaturized lumped-distributed balun for modern wireless communication systems," in *Proc. IEEE Midwest Circuits and Systems Symp.*, vol. 3, 1996, pp. 1347–1350.
[12] B. P. Kumar, G. R. Branner, and B. Huang, "Parametric analysis of improved planar balun circuits for wireless microwave and RF applications," in *Proc. IEEE Midwest Circuits and Systems Symp.*, 1998, pp. 474–475.
[13] C. W. Tang and C. Y. Chang, "A semi-lumped balun fabricated by low temperature co-fired ceramic," in *IEEE MTT-S Int. Microwave Symp. Dig.*, 2002, pp. 2201–2204.
[14] Y. C. Leong, K. S. Ang, and C. H. Lee, "A derivation of a class of 3-port baluns from symmetrical 4-port networks," in *IEEE MTT-S Int. Microwave Symp. Dig.*, 2002, pp. 1165–1168.
[15] G. L. Matthaei, L. Yong, and E. M. T. Jones, *Microwave Filters, Impedance Matching Networks and Coupling Structures*. New York: McGraw-Hill, 1964, pp. 217–229.
[16] S. A. Maas and K. W. Chang, "A broadband planar, doubly balanced monolithic $K\acute{a}$-band diode mixer," *IEEE Trans. Microwave Theory Tech.*, vol. 41, pp. 2330–2335, Dec. 1993.

**Kian Sen Ang** (M'02) was born in Singapore, in 1969. He received the B.Eng. degree from the National University of Singapore, Singapore, in 1994, and the Ph.D. degree from the University of Surrey, Surrey, U.K., in 2000.

In 1994, he joined the DSO National Laboratories, Singapore, as a Research Engineer involved in microwave circuit and sub-system designs. He is currently a Senior Member of Technical Staff with the DSO National Laboratories. His research interests include design, analysis, and measurement of novel microwave circuits including monolithic integrated circuits. He has authored over 20 publications in this area and was a contributing author of *RFIC and MMIC Design and Technology* (London, U.K.: IEE Press, 2001).

**Yoke Choy Leong** received the B.Eng. (with honors) and M.Sc. degrees from the National University of Singapore, Singapore, in 1991 and 1995, respectively, and the Ph.D. degree from the University of Massachusetts at Amherst, in 2000.

Since 1991, he has been with the DSO National Laboratories, Singapore, where he is involved in the area of microwave component and system design. His research interest is in microwave/millimeter-wave MMIC design and modeling, analysis, and synthesis of novel passive structures.

**Chee How Lee** was born in Singapore, in 1975. He received the M.Eng. degree from the Imperial College of Science, Technology and Medicine, London, U.K., in 1998.

Since 2001, he has been an Engineer with DSO National Laboratories, Singapore, where he has been involved in microwave component and sub-system design. His research interest is in the design, analysis, and synthesis of microwave MMIC and novel passive structures.